Sadi, Toufik; Kivisaari, Pyry; Oksanen, Jani; Tulkki, Jukka

On the correlation of the Auger generated hot electron emission and efficiency droop in III-N light-emitting diodes

Published in:
Applied Physics Letters

DOI:
10.1063/1.4894862

Published: 01/09/2014

Document Version
Publisher's PDF, also known as Version of record

Please cite the original version:
Sadi, T., Kivisaari, P., Oksanen, J., & Tulkki, J. (2014). On the correlation of the Auger generated hot electron emission and efficiency droop in III-N light-emitting diodes. *Applied Physics Letters*, *105*(9), 1-5. Article 091106. https://doi.org/10.1063/1.4894862

On the correlation of the Auger generated hot electron emission and efficiency droop in III-N light-emitting diodes

Toufik Sadi, Pyry Kivisaari, Jani Oksanen, and Jukka Tulkki

Citation: Appl. Phys. Lett. **105**, 091106 (2014); doi: 10.1063/1.4894862
View online: https://doi.org/10.1063/1.4894862
View Table of Contents: http://aip.scitation.org/toc/apl/105/9
Published by the American Institute of Physics

On the correlation of the Auger generated hot electron emission and efficiency droop in III-N light-emitting diodes

Toufik Sadi, Pyry Kivisaari, Jani Oksanen, and Jukka Tulkki
Department of Biomedical Engineering and Computational Sciences, Aalto University, P.O. Box 12200, FI-00076 Aalto, Finland

(Received 21 July 2014; accepted 26 August 2014; published online 3 September 2014)

Recent experiments presented in by Iveland *et al.* [Phys. Rev. Lett. **110**, 177406 (2013)] demonstrated that hot electron emission from cesiated *p*-contacts of III-nitride quantum-well (QW) light-emitting diodes (LEDs) coincides with the onset of the efficiency droop. We have carried out Monte Carlo simulations of hot-electron transport in realistic III-N LEDs. The simulations account for the hole population and all relevant electron scattering and recombination processes. We show that Auger recombination generates a significant hot electron population, which is temporarily trapped in the conduction band side-valleys, without decaying completely before reaching the *p*-contact. The leakage current due to electron overflow and thermal escape from the QWs is shown to have a minimal impact on the droop. We conclude that the experimentally observed hot electrons are created by Auger recombination in QWs, and that the Auger effect as the origin of the droop is the only consistent explanation for the experimental findings of Iveland *et al.*, [Phys. Rev. Lett. **110**, 177406 (2013)]. © *2014 AIP Publishing LLC*. [http://dx.doi.org/10.1063/1.4894862]

The detailed origin of the efficiency droop, which seriously limits the performance of modern III-N light-emitting diodes (LEDs), has remained a topic of constant debate for over a decade. Auger recombination[1–4] and electron leakage[5] have been commonly suggested as the main causes of the droop, but a widely accepted evidence on its origin has been missing. Very recently, however, Iveland and co-workers reported promising experimental results, where the emission of very high-energy electrons from the surface of a cesiated *p*-contact of a III-N quantum-well (QW) LED correlates perfectly with the onset of the droop.[1] Based on this correlation discovery, they concluded that Auger recombination is the fundamental origin of the droop. Soon after the reports in Ref. 1, the importance of hot carriers was also detected in low temperature photoluminescence measurements,[4] where high-energy photoluminescence in structures with alternating blue and green QWs was shown to result from Auger-generated hot carriers and was found to correlate with the onset of the droop. However, the origin of the hot carriers and its detailed relation to the droop has created a dynamic debate within the LED community, and undoubtedly results in a renewed interest in theoretical work related to device level simulations of charge transport and carrier dynamics.

In this letter, we report microscopic Monte Carlo (MC) simulations of electron transport in III-N LEDs, to clarify the relation between Auger recombination, the efficiency droop, and the hot-electron spectra observed in Ref. 1. The simulations use the MC approach to describe the full spectrum of the scattering, recombination and non-equilibrium transport effects of the electron system, and a quasi-equilibrium transport model to describe the hole system. The simulations are carried out to answer two questions: (1) does Auger recombination in the QWs result in a sufficiently large hot electron population to explain the hot electron emission at the *p*-contact measured in Ref. 1 and (2) what are the roles of the non-radiative Auger recombination in the QWs and the *p*-contact electron leakage current in determining the efficiency droop?

To create a conclusive and quantitative link between the droop, Auger recombination in the QWs and the hot electron emission at the semiconductor surface, one needs fully microscopic device-level simulations of non-equilibrium transport in realistic III-N LEDs, in addition to reliable models for Auger recombination and other scattering rates. With the exception of microscopic models restricted to carrier dynamics within the QWs,[6] earlier simulations have relied heavily on quasi-equilibrium models, e.g., the drift-diffusion (DD) model,[7–11] which do not account for hot electrons at high input powers. To describe hot electrons and to maintain computational feasibility, we have combined the MC and DD methods. We study the one dimensional (1D) multi-quantum well (MQW) wurtzite c-plane III-N LED shown in Fig. 1, which also illustrates the transport mechanisms governing III-N LED operation. The total distance between the topmost QW and the *p*-contact is essentially the same as in the QW structure studied experimentally in Ref. 1, and is ∼250 nm. As almost all the recombination in III-N MQW LEDs takes place in the QW closest to the *p*-contact,[12] this distance is the most important factor affecting electron transport through the *p*-GaN layer in the LED.

The Monte-Carlo-drift-diffusion (MCDD) method used here is based on combining the MC method of solving the Boltzmann transport equation and the DD model, to create an advanced physical model describing electron transport in modern LEDs. As a first step, we use the DD model to calculate the position-dependent electron (n) and hole (p) densities, as well as the electrostatic potential.[9] In contrast to the MC model, the DD model only considers the lowest Γ_1 valley within the parabolic approximation. The DD simulation parameters, including the hole and electron effective masses, the valence and conduction band discontinuities, permittivities, and mobilities are given in Ref. 9. Polarization parameters are based on first-principle calculations.[13] The interband recombination rates in the DD equations depend on n and p through the ABC model relating the Shockley-Read-Hall

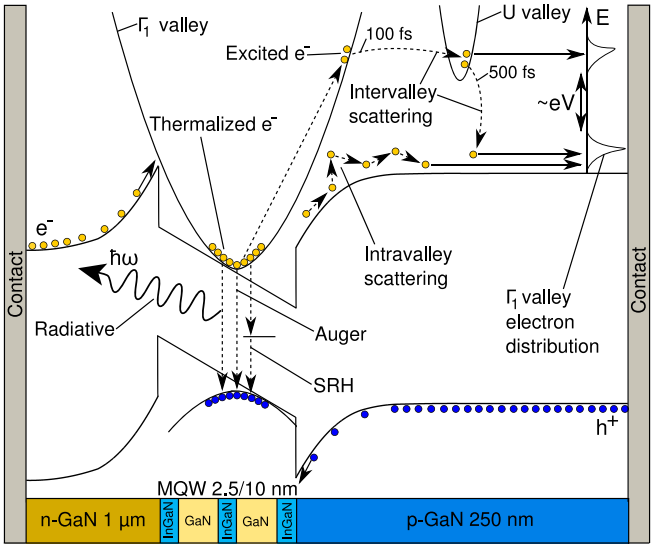

FIG. 1. A schematic illustration of the studied LED and the transport mechanisms governing its operation, including band-to-band recombination, intraband scattering and *p*-contact electron leakage.

(SRH), radiative and Auger recombination rates to carrier densities.[14] These rates are calculated using the electron and hole SRH lifetimes $\tau_n = \tau_p = 10^{-7}$s, the net radiative recombination coefficient $B = 4 \times 10^{-17}$ m^{3}s^{-1}, and the Auger coefficients for electrons and holes $C_n = C_p = 10^{-42}$ m^{6}s^{-1}, in accordance with empirical values from Refs. 11 and 15.

The MC simulation step describes the time evolution of the positions and momenta of a very large number (~millions) of electrons, moving in an electric field that is self-consistently updated by regularly solving Poisson's equation (every 1 fs). The electron trajectories follow classical mechanics while accounting for the details of the bandstructure and the multiple scattering, recombination, and generation processes. MC simulations are run for a lattice temperature of 300 K until a steady state is reached (typically after tens of nanoseconds of device operation). The DD hole density is used as a fixed background charge in the MC simulation, and the DD electron distributions and recombination rates are used as initial values to achieve fast MC convergence.

In the MC simulations, we use the spherical nonparabolic five-valley electron bandstructure model of wurtzite GaN described in Ref. 16. This model is an analytical fit to the full bandstructure calculation presented in,[17] based on empirical pseudopotentials fitted to reproduce experimental data. The conduction band minimum is located at the Γ-point in the central valley Γ_1. The lowest satellite valleys occur at the six equivalent *U*-points, which are located at two thirds of the way between the *L*- and *M*-points. Additional higher valleys in the conduction band occur at the Γ- (the Γ_3 valley), the three equivalent *M*- and the two equivalent *K*-points. The *U*, Γ_3, *M*, and *K* valleys are located 1.49, 1.75, 2.15, and 2.6 eV above the Γ-point minimum, respectively. The electron energy-wavevector dispersion in each valley is described by $E_d(1 + \alpha E_d + \beta E_d^2) = \hbar^2 k^2 / 2m^*$, where m^* is the electron effective mass, α and β are the nonparabolicity constants, and E_d and k are the energy and momentum, respectively, measured with respect to the values at the bottom of each valley. The effective masses of the lowest Γ_1 and *U* valleys, which are most relevant in our simulations, are $0.2m_0$ and $0.33m_0$, respectively, and the corresponding nonparabolicity factors α/β are $0.19\,\text{eV}^{-1}/0.08\,\text{eV}^{-2}$ and $0.17\,\text{eV}^{-1}/0\,\text{eV}^{-2}$. The bandstructure of $In_{0.15}Ga_{0.85}N$ is GaN-like, and is obtained using linear or second-order interpolation between the GaN bandstructure[16] and the InN bandstructure (also originating from semi-empirical pseudopotential methods).[18] Important InN parameters include the bandgap and the Γ_1 effective mass of 0.77 eV and $0.11m_0$, respectively. Additional basic GaN and InGaN parameters are given in Ref. 9.

The MC simulation accounts for all important intravalley and intervalley electron-phonon scattering mechanisms. Intravalley phonon scattering is either of a deformation potential type, caused by low-energy acoustic and 92 meV longitudinal optical (LO) phonons, or of a piezoelectric type (negligible at 300 K). The intervalley phonon-assisted scattering processes included in the simulations are of the deformation potential type and are caused by 65 meV optical phonons. Furthermore, the model accounts for ionized impurity scattering due to dopants, alloy disorder scattering in the QWs, electron-electron, and electron-hole Coulomb interactions, as well as the recombination and generation of electron-hole pairs by SRH, radiative and Auger processes. The scattering parameters and the transition rate expressions for the mechanisms involving various intermediate phonon, photon and hole states, as derived from Fermi's Golden Rule, are well-documented in literature for the bandstructures used in this work.[16,19,20] Further details on how MC electron transport simulations are carried out in III-N devices can be found in Refs. 21 and 22.

Interband Scattering. To include interband processes at the same level of accuracy as intraband processes, we would need the annihilation probabilities $P(\mathbf{k})$ of the electrons and the high-energy generation probabilities $P(\mathbf{k}, \mathbf{k}')$ related to Auger processes ($\mathbf{k}$ and $\mathbf{k}'$ are the wavevectors of the initial and final states of the excited electron). The inclusion of interband scattering in ensemble MC calculations is therefore challenging due to the uncertainties in the interband rates available from theoretical and experimental data.[23,24] However, we can obtain semi-quantitative estimates for the interband rates from the available total recombination rates obtained from semi-empirical ABC parameterization by (1) assuming that all carriers within a narrow (a few k_BT) energy range near the bottom of the conduction band (where the majority of the carriers are located and recombination events predominantly occur) have an equal recombination probability, and (2) using energy conservation laws to determine the corresponding energy range of the final states of Auger excited electrons, whose probabilities are also assumed to be independent of the wavevectors due to the predominant nature of phonon-assisted Auger recombination processes in III-N semiconductors.[23] These assumptions result in a simple model where the rates obtained from the ABC model are used to randomly annihilate electrons within 100 meV from the conduction band minimum. The Auger rates of hot electron generation are then given by the total indirect CHCC Auger recombination rate $C_n pn^2$,[25] which is used to excite random electrons within the 100 meV band to random states

in the conduction band, whose energies are approximately equal to the sum of the initial state and bandgap energies. The chosen 100 meV band represents a conservative estimate for the thermal and lifetime broadening expected in the QWs. In the MC simulations, we use the same ABC coefficients employed in DD simulations.[11] The used Auger coefficients are comparable to values obtained from first-principle calculations.[23] The recombination rates are self-consistently updated using the MC electron densities.

To establish the relationship between Auger recombination and the hot electron population at the *p*-contact surface, we map out and study the electron distribution function as a function of energy and the distance from the MQW stack in the *p*-GaN layer, for current densities corresponding to weak and strong Auger recombination in the QWs. Figure 2(a) shows the distribution function map for strong current injection ($J = 400\ \mathrm{A/cm^2}$), where the external quantum efficiency (EQE) has dropped from the maximum 0.62 to 0.5. As can be seen, there is a considerable high-energy electron population leaking to the *p*-GaN, but also a large number of electrons near the 1.5 eV energy, which corresponds to the bottom of the upper *U*-valley. The trapping of electrons in the *U*-valley results in a visibly increased hot electron population all the way to the surface of the *p*-contact. However, the population becomes gradually smaller towards the *p*-contact, as the hot electrons are scattered to the Γ_1 valley and subsequently quickly relax towards the Γ_1 minimum. The relaxation towards the Γ_1 minimum is dominated by phonon scattering described by energy-dependent rates resulting in average electron state lifetimes of ~10 fs. The lifetimes of the phonon-mediated intervalley electron transitions from the *U* valleys to the Γ_1 valley and the relevant high-energy Γ_1 valley states to the *U* valleys are on average ~500 fs and ~100 fs, respectively, in agreement with experimental values.[26]

Fig. 2(b) shows a more detailed comparison of the distribution functions next to the *p*-contact for weak and strong injections. Fig. 2(b) indicates that, for all bias voltages, the distribution function at energies above 0.2 eV is clearly different from a quickly decaying distribution function corresponding to quasi-equilibrium. However, visible trapping of electrons in the *U*-valley only starts when the current density exceeds $J = 5\ \mathrm{A/cm^2}$. The trapped electron density at the *U*-valley also increases roughly by 3–4 orders of magnitude when the current density increases from 5 A/cm^2 to 400 A/cm^2. Figure 2(c) complements the data in Figs. 2(a) and 2(b) by showing the current density and the EQE as a function of the bias voltage. Comparison to Fig. 2(b) shows that the observed side-valley population starts to appear at the current density coinciding with the onset of the droop. Analysis of Fig. 2 therefore gives a direct theoretical demonstration that *hot electron generation in the QWs explains the high-energy electron emission from the p-contact observed experimentally in* Ref. 1.

Figures 3(a) and 3(b) show the conduction band edge energy for weak ($V = 3\ \mathrm{V}$, $J = 20\ \mathrm{A/cm^2}$) and strong ($V = 3.3\ \mathrm{V}$, $J = 400\ \mathrm{A/cm^2}$) injection, and present a comparison with the results obtained from the DD model. The MCDD and DD predictions deviate only slightly from each other at 3 V, but at 3.3 V the deviation is already quite significant in and near the MQWs, as hot electrons start to affect the carrier densities. To further elaborate on the origin of the hot electrons, we show in Fig. 3(c) the average electron

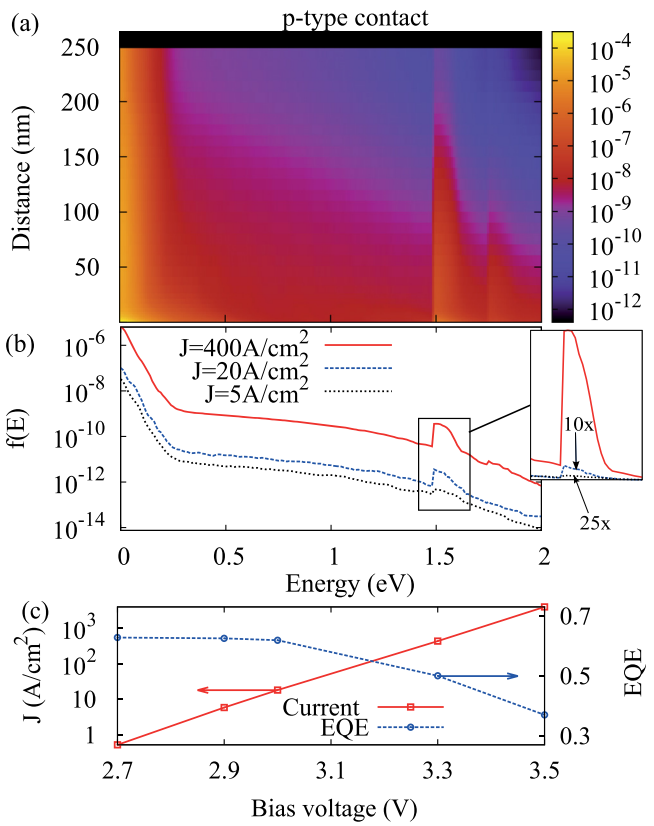

FIG. 2. (a) The electron distribution function $f(E, y)$ in the *p*-GaN layer as a function of energy E and distance y from QWs, for strong injection ($J = 400\ \mathrm{A/cm^2}$). (b) The electron distribution functions $f(E, 250\ \mathrm{nm})$ for weak injection around onset of the droop ($J = 5\ \mathrm{A/cm^2}$ and $J = 20\ \mathrm{A/cm^2}$) and for strong injection ($J = 400\ \mathrm{A/cm^2}$). The inset shows $f(E, 250\ \mathrm{nm})$ in a linear scale, around the *U*-valley minimum energy (1.5 eV). (c) The current density J and the EQE (right axis), calculated assuming an extraction efficiency of 0.75, as a function of the bias voltage.

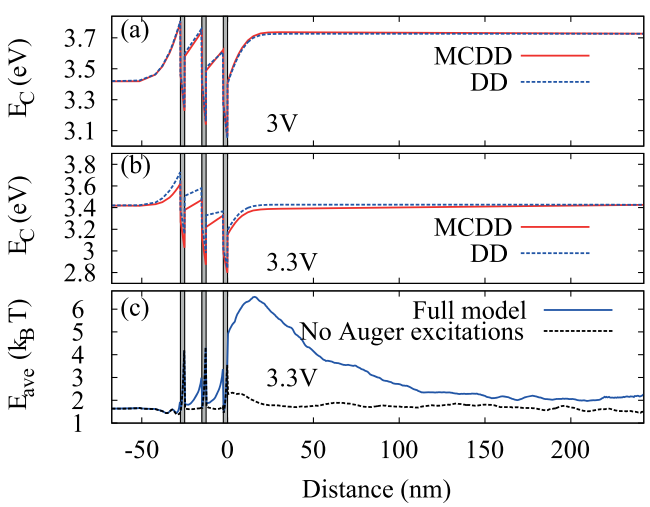

FIG. 3. The conduction band edge energy E_C at (a) weak and (b) strong injections, calculated from MCDD and DD methods. (c) Average electron energy ($E_{ave} = E - E_{\Gamma_1}$), for strong injection (3.3 V) with and without Auger excitations, using the MCDD method. Energies E_C and E_{ave} are shown as a function of the distance from the top of the MQW stack. The *n*-GaN ($y < -27.5\ \mathrm{nm}$) and *p*-GaN ($y > 0\ \mathrm{nm}$) layers, and the QWs (in gray) are included in the figure (see Fig. 1).

energy with respect to the minimum of the Γ_1 valley, as a function of the distance from the top of the MQW stack for $V = 3.3$ V. Fig. 3(c) shows two energy curves, calculated using the full model and a model where the excitation of electrons by the Auger processes has been disregarded. In the latter case, practically no hot electrons leak to the *p*-GaN layer, resulting in an average energy of $\sim 1.5 k_B T$ almost everywhere in the *p*-GaN layer. With the full model, however, the average electron energy increases to $6 k_B T$ due to the Auger excitation, although the average energy quickly decreases further away from the QWs due to multiple inelastic lattice collisions and intervalley scattering. The high average energy shows that *the Auger excitation alone is responsible for generating the high-energy electrons observed in* Fig. 2.

Figure 4 shows the total LED current, the current component resulting from Auger recombination in the QWs, and the total electron leakage current through the *p*-contact with and without Auger excitations, as a function of the bias. The contribution of the Auger current to the total current increases throughout the bias range, eventually forming 40% of the total current at $V = 3.5$ V. The leakage current on the other hand is at most 5% of the total current, and the Auger-excited electrons contribute to up to 90% of the leakage current. These results indicate that *electron transport effects, which are fully accounted for by the present model, cannot explain the droop by themselves*. Together, the presented results lead to an important conclusion: the efficiency droop is caused by the Auger effect through the annihilation of electrons via nonradiative recombination. While the leakage of the hot electrons through the *p*-contact is a signature of the efficiency droop, the impact of this loss mechanism on the droop itself is minimal.

Previous MC simulation[27] of the transport of hot electrons through a *p*-GaN barrier suggested that the hot electrons measured in Ref. 1 cannot originate from Auger recombination in the QWs. However, the simulations in Ref. 27 only describe transport in the barrier layer, and force the electron distribution at the MQW–*p*-GaN interface to be located 3 eV above the conduction band minimum. This is in contrast to our MCDD model, where the results are calculated self-consistently for a full device under a range of bias voltages, with the whole electron distribution reflecting steady-state operating conditions. Furthermore, detailed comparison and analysis of the results of Ref. 27 is not possible due to the very concise presentation of the results. The predictivity of our calculated MC hot-electron distribution depends mainly on the accuracy of the III-N parameters and intraband and interband scattering rates. If we use different parameters within the range of published III-N data, the conclusions on side-valley transport and Auger-related leakage currents still hold, although the quantitative details in the results will change. The semi-empirical bandstructure parameters used here, mainly the effective masses, nonparabolicities, and satellite valleys energy separations, are within the range of commonly reported values. Using more sophisticated full-band models is not expected to provide significantly more accurate predictions, due to the large uncertainties present in these models. The intraband and interband scattering rates have been extracted from semi-empirical data, using the well-established formalism adopted widely in III-N device simulations.[11,15,20–23]

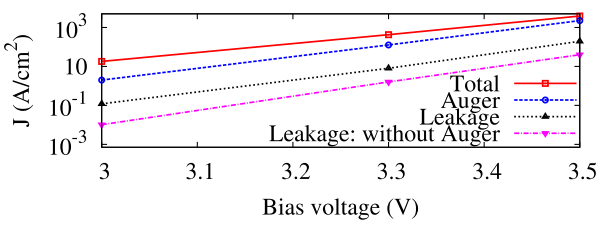

FIG. 4. The total and Auger currents, and the *p*-contact leakage current with and without Auger excitations, as a function of the bias.

The results presented here do not account for hot hole generation through Auger processes. Although hot holes are not observable in the measurement setup used in Ref. 1, they can affect LED efficiency by introducing additional leakage current channels.[4] However, due to their much lower mobility in III-nitrides and the longer distance to the n-contact in typical III-N LEDs, we expect the contribution of hot holes to carrier leakage to be notably smaller than that of electrons, even if their generation rate is equal to the electron generation rate. Studying the hot hole effect is therefore out of the scope of this work.

In comparing our results with Ref. 1, one must further note that the LED of Ref. 1 includes an electron blocking layer (EBL). While using an EBL may reduce the direct current flow, we do not expect that using an EBL will significantly affect our conclusions. This is because the Auger generated high-energy electrons have sufficient energy to overcome the potential barriers created by the EBL located right next to the QWs.

In conclusion, we have used detailed electron transport simulations to show that Auger recombination in the QWs is the fundamental cause of the hot electron emission recently observed by Iveland *et al.* in III-N LEDs.[1] Our simulations are able to account for electron transport and related scattering mechanisms under realistic conditions at the device level. The results show how the hot electron population created by Auger recombination in the QWs is trapped in the high-energy side-valleys and transported to the semiconductor surface through a p-type barrier layer. In addition to demonstrating in detail the relationship between Auger recombination and the non-local hot electron population, our results also show that electron overflow from the QWs or other current leakage mechanisms cannot cause the droop. This strongly indicates that Auger recombination alone is responsible for the efficiency droop in III-N LED structures.

We acknowledge support from the Academy of Finland and the Aalto energy efficiency research programme.

[1]J. Iveland, L. Martinelli, J. Peretti, J. S. Speck, and C. Weisbuch, Phys. Rev. Lett. **110**, 177406 (2013).
[2]Y. C. Shen, G. O. Mueller, S. Watanabe, N. F. Gardner, A. Munkholm, and M. R. Krames, Appl. Phys. Lett. **91**, 141101 (2007).
[3]A. Olsson, A. Aierken, J. Oksanen, S. Suihkonen, H. Lipsanen, and J. Tulkki, Appl. Phys. Lett. **102**, 081123 (2013).
[4]M. Binder, A. Nirschl, R. Zeisel, T. Hager, H.-J. Lugauer, M. Sabathil, D. Bougeard, J. Wagner, and B. Galler, Appl. Phys. Lett **103**, 071108 (2013).

[5]G.-B. Lin, D. Meyaard, J. Cho, E. F. Schubert, H. Shim, and C. Sone, Appl. Phys. Lett. **100**, 161106 (2012).
[6]I.-L. Lu, Y.-R. Wu, and J. Singh, Phys. Status Solidi C **8**, 2393 (2011).
[7]K. A. Bulashevich, V. F. Mymrin, S. Y. Karpov, I. A. Zhmakin, and A. I. Zhmakin, J. Comput. Phys. **213**, 214 (2006).
[8]X. Ni, Q. Fan, R. Shimada, Ü. Özgür, and H. Morkoc, Appl. Phys. Lett. **93**, 171113 (2008).
[9]P. Kivisaari, J. Oksanen, and J. Tulkki, J. Appl. Phys. **111**, 103120 (2012).
[10]P. Kivisaari, J. Oksanen, and J. Tulkki, Appl. Phys. Lett. **103**, 211118 (2013).
[11]J. Piprek and Z. M. S. Li, Appl. Phys. Lett. **102**, 023510 (2013).
[12]A. David, M. J. Grundmann, J. F. Kaeding, N. F. Gardner, T. G. Mihopoulos, and M. R. Krames, Appl. Phys. Lett. **92**, 053502 (2008).
[13]F. Bernardini and V. Fiorentini, Phys. Rev. B **64**, 085207 (2001).
[14]O. Heikkilä, J. Oksanen, and J. Tulkki, J. Appl. Phys. **107**, 033105 (2010).
[15]A. David and M. J. Grundmann, Appl. Phys. Lett **96**, 103504 (2010).
[16]J. D. Albrecht, R. P. Wang, P. P. Ruden, M. Farahmand, and K. F. Brennan, J. Appl. Phys. **83**, 4777 (1998).
[17]R. Wang, P. P. Ruden, J. Kolnik, I. Oguzman, and K. F. Brennan, J. Phys. Chem. Solids **58**, 913 (1997).
[18]F. Bechstedt, J. Furthmüller, M. Ferhat, L. K. Teles, L. M. R. Scolfaro, J. R. Leite, V. Y. Davydov, O. Ambacher, and R. Goldhahn, Phys. Status Solidi A **195**, 628 (2003).
[19]B. K. Ridley, *Quantum Processes in Semiconductors*, 4th ed. (Clarendon Press, 1999).
[20]C. Jacoboni and L. Reggiani, Rev. Mod. Phys. **55**, 645 (1983).
[21]T. Sadi, R. W. Kelsall, and N. J. Pilgrim, IEEE Trans. Electron Devices **53**, 2892 (2006).
[22]T. Sadi and R. W. Kelsall, IEEE Electron Device Lett. **28**, 787 (2007).
[23]E. Kioupakis, P. Rinke, K. T. Delaney, and C. G. V. de Walle, Appl. Phys. Lett. **98**, 161107 (2011).
[24]M. Brasken, M. Lindberg, M. Sopanen, H. Lipsanen, and J. Tulkki, Phys. Rev. B **58**, R15993(R) (1998).
[25]A. Haug, Appl. Phys. A **51**, 354 (1990).
[26]S. Wu, P. Geiser, J. Jun, J. Karpinski, D. Wang, and R. Sobolewski, J. Appl. Phys. **101**, 043701 (2007).
[27]F. Bertazzi, M. Goano, X. Zhou, M. Calciati, G. Ghione, M. Matsubara, and E. Bellotti, "Comment on 'Direct Measurement of Auger Electrons Emitted from a Semiconductor Light-Emitting Diode under Electrical Injection: Identification of the Dominant Mechanism for Efficiency Droop'," e-print arXiv:1305.2512v3 (2013).